Modeling and Performance Evaluation of a Hybrid Solar-Wind Power Generation Plant

Emeghara, M.C[a], Obi, P.I[*b], and Onah, A.J[b]

[a]Department of Electrical and Computer Engineering, Tennessee Technological University, Cookeville, TN, USA
[b]Department of Electrical/Electronic Engineering, Michael Okpara University of Agriculture, Umudike, Abia State, Nigeria.
Corresponding Author Email: patndyobi@gmail.com

Article Information

Abstract

This research presents a comprehensive modeling and performance evaluation of hybrid solar-wind power generation plant with special attention on the effect of environmental changes on the system. Unlike fossil fuels, renewable energy sources possess inherent intermittent nature that limits their stable power supply, but by combining two or more renewable sources to form a hybrid unit, the individual limitations are over come since they can complement each other. Also, the main problem of renewable hybrid system is optimal sizing; oversized system is uneconomical while under sized can lead to failure of power supply or insufficient power delivery. However, in order to select an optimum combination for hybrid renewable energy system to meet the load demand, the modeling and performance evaluation of the individual components of a hybrid solar-wind energy system as well as the entire system was carried out in this paper using mechanistic method in which the physical laws and theories of the individual subsystems of the system under study were analyzed considering their respective mathematical models. More so, results from the simulation of a 37.8 V solar module shows that changes in irradiance and temperature affect greatly the power output of the PV module for both ideal and non-ideal single diode models, while changes in wind speed affect the output power of the 1575 W wind turbine under study. In addition, the hybrid solar-wind power system results show a geometrical increase in power output when compared to the individual subsystems. The hybrid performance evaluation under different varying environmental factors show that increase in irradiance and wind velocity has a more significant impact on the hybrid system than temperature changes.

1. Introduction

Energy is essential to our society to ensure our quality of life and to underpin all other elements [1, 2]. The demand for electrical energy stimulated by the relative ease with which electricity can be generated, distributed, and utilized, and by the great variety of its applications has developed largely across the whole world; in every country and society we live. However, electricity can be generated primarily either from renewable or non-renewable energy resources, in which over 65% of the world's electrical energy used today is generated through non-renewable sources (fossil fuels and nuclear fuel). Continuous usage of these conventional resources to meet the growing demand of electricity have resulted in increased energy crisis and the pollutants created from the burning of the

conventional resources cause respiratory illnesses and death in humans and destroy fragile ecosystem [3]. Also, relying entirely on non-renewable resource; electricity generation is a risk in the future as they are finite sources. Thus, the way forward is to exploit more the use of renewable sources for continuous electricity generation.

Renewable energy sources such as wind, hydro, solar, biomass, geothermal, etc, are better alternatives to conventional energy sources, but they are less competitive due to their uncertainty and high initial cost [4, 5]. Also, the generation of electricity from these renewable sources is dependent on weather condition and possess inherent intermittent nature, which hinders stable power supply [6], and makes integration to micro-grid difficult, especially if the local grid is not connected to the main grid. However, the integration of two or more renewable energy systems to form a hybrid unit can serve as a permanent solution [7] to the random variability associated more with the individual sources, because the sources can complement each other to provide higher quality and more reliable power to consumers than the individual source system.

Although hybridization of different renewable sources can complement each other to some extent and achieve higher total energy efficiency, but there exist the problem of optimal sizing; over sizing the system components will enhance the system cost whereas under sizing can lead to failure of power supply or insufficient power delivered to the load [8]. Sizing is of utmost importance to the modeling and operation of a hybrid solar-wind power generation. Sizing has to be optimal in modeling to achieve a preferred level of reliability at the smallest probable cost. Several methods have been adopted or employed by different scholars in their respective studies or researches which include, hourly collection of data of both wind speed and solar radiation, graphical construction, downhill simplex and multi-objective optimal unit sizing [9a,10a]. However, in order to select an optimum combination for hybrid renewable energy system to meet the load demand, the modeling and performance evaluation of the individual components as well as the entire system is of great essence. Therefore, this research work is focused on studying the modeling and performance evaluation of a hybrid solar-wind power system.

Renewable resources are often located in remote areas, and it can be expensive to build power line to the cities where the electricity produced is needed most [11].

More so, renewable sources are limited by the fact that they are not always available, for instance, cloudy days reduce electricity generated from solar installations; days without wind reduces electricity from wind farms; and droughts or lean flow reduces the water available for hydropower. But by hybridizing two or more renewable sources, the individual limitations are overcome.

Figure 1 shows the block diagram of a typical hybrid solar-wind power system. The power supplied by the solar and wind system is centralized on a direct current (DC) bus. The output of the solar system is connected through a boost DC-DC converter to the DC bus, while the wind turbine output which is alternating current (AC) is further converted to DC, and then connected to the DC bus. Also, the respective output of these sources are made to charge a storage system (batteries) which is designed to supply DC power to the DC bus in case a shortfall in weather condition cause either of the sources to temporarily stop generating. However, the three power inputs to the DC bus (from solar, wind and storage system) are multiplexed to an output that can either serve directly a DC load or further converted to AC through an inverter for further distribution.
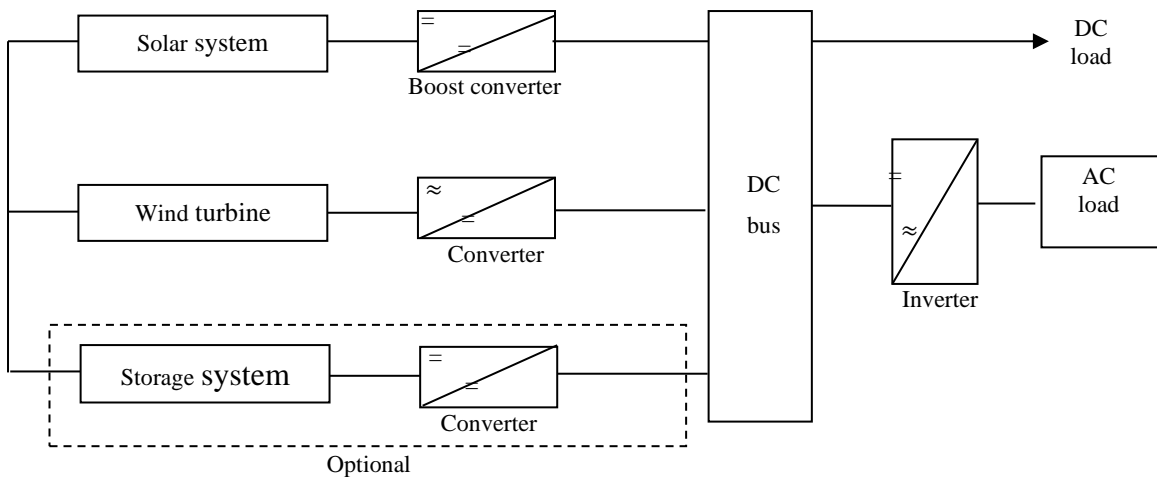
Figure 1: Hybrid solar-wind power system

2. Methodology

In order to sufficiently model and evaluate the influence of different environmental factors affecting the performance of a hybrid solar-wind power system such as variations in wind speed, Irradiance and Temperature, it is imperative to review in this section the materials and methods adopted in the analysis of this research.

2.1 Materials

The following materials were used in the simulation of this research work:
- Mitsubishi electric PV module manufacturer's datasheet; attached as Appendix 2.
- Pika T701 wind turbine installation and service manual; attached as Appendix 1.
- Matlab software
- Laptop computer system with the following system properties; HP, intel processor, 2.30 Hz, 4.0 GB, 64 bit.

2.2 Methods

The hybrid renewable system under discussion consists of two energy conversion components: the PV Module and wind turbine, as well as a storage device (battery). The working together of these components though with different inhibiting factors can guarantee a stable power supply to a large extent. However, in order to correctly select the components and subsystems of a hybrid renewable solar-wind power system for optimal sizing of the entire system, the most important step was the modeling of its individual components. This was achieved by using mechanistic method [12, 13] in which the physical laws and theories of the individual subsystems of the proposed hybrid solar-wind power system were analyzed considering their individual mathematical models.

2.2.1 PV cell mathematical modeling

The building block of a PV cell is synonymous to the principle of operation a p-n junction semi-conductor. It consists of a silicon p-n junction capable of releasing electrons around a closed electrical circuit when exposed to light using photovoltaic effects. By using the principle of photovoltaic effects [14, 15], a physical interpretation of the equivalent circuit of a solar cell can be modeled through the circuits shown in Figures 2, 3 and 4. When sunlight hits the cell, photons are absorbed by the p-n junction atoms, thus, freeing electrons from the n-type or n-doped layer. These

electrons are then free to move across the junction due to the built-in potential and create a current. Hence, this is modeled by the light generated current source, I_{Ph}. The intrinsic silicon p-n junction characteristic is simulated as a diode in the circuit equivalent. During darkness, the solar cell is not an active device; it works as a diode, i.e. a p-n junction. It produces neither current nor voltage. This shows that the output of the current source is directly proportional to the light falling on the cell (photocurrent). Thus, the photon generated current source I_{Ph} is in fact related with solar irradiance.

For the purpose of this study, only the ideal and non-ideal PV cell single diode model [16] was considered. However, the parameters of the PV cells considered were evaluated using classical circuit theory for each equivalent model connection.

➤ *Ideal single diode photovoltaic model*

An ideal photovoltaic cell consists of a single diode connected in parallel with a light generated current source, I_{Ph} as shown in Figure 2.
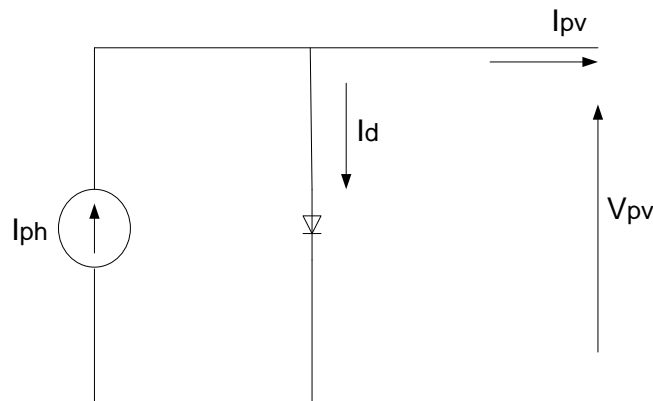
Figure 2: Equivalent single diode circuit model for ideal PV cell [17].

The output current, I_{PV}, is deduced as follows:

$$I_{PV} = I_{Ph} - I_d \tag{1}$$

Where,

I_{PV} = Output current,

I_{Ph} = Light generated current, and

I_d = Diode current

According to [17], the current through a p-n junction diode is given as;

$$I_d = I_S \left[\exp\left(\frac{V}{nV_T}\right) - 1 \right] \tag{2}$$

Therefore,

$$I_{PV} = I_{Ph} - I_S \left[\exp\left(\frac{V}{nV_T}\right) - 1 \right] \tag{3}$$

Where,

V = Output voltage

I_S = Cell saturation of dark current,

V_T = Thermal voltage

Also, according to [16], the thermal voltage is given as;

$$V_T = \frac{KT_c}{q} \tag{4}$$

K = Boltzmann's constant = $1.3806503 \times 10^{-23}$ J/K

T_c = Cell operating temperature (in Kelvin)

q = Electron charge = $1.60217646 \times 10^{-19}$ C

n = Ideality factor = 1.3

➤ *Non-ideal photovoltaic model*

The non-ideal model is made up of photovoltaic cell with series resistance and photovoltaic with series and parallel resistance.

The photovoltaic model with series resistance (R_S - model) shown in Figure 2 was achieved with the inclusion of a series resistance R_S, which represents the circuit internal resistance.
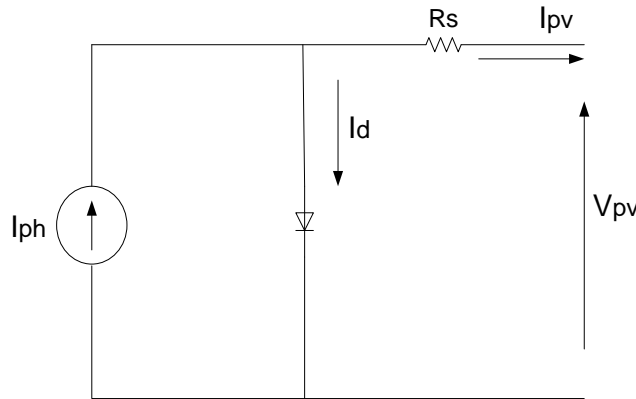
Figure 3: Equivalent model circuit of single diode PV cell with series resistance [18].

The output current is deduced as follows:
$$I_{PV} = I_{Ph} - I_d \tag{5}$$
Where,
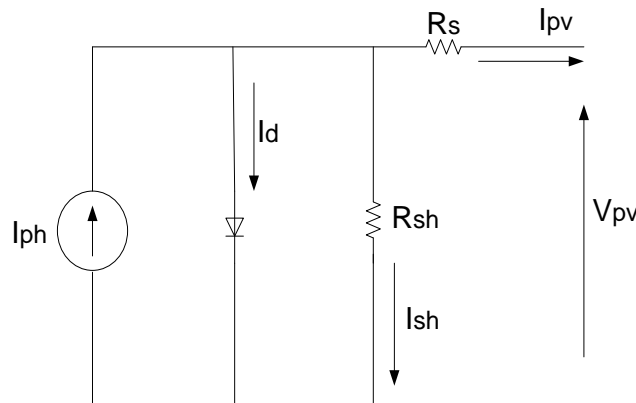$$I_d = I_S \left[\exp\left(\frac{V + I_{PV}R_S}{nV_T} \right) - 1 \right] \tag{6}$$
Therefore,
$$I_{PV} = I_{Ph} - I_d = I_{Ph} - I_S \left[\exp\left(\frac{V + I_{PV}R_S}{nV_T} \right) - 1 \right] \tag{7}$$
Where,
R_S = Series resistance.

The introduction of the parallel resistance is based on the fact that Equation (7) cannot effectively represent the behavior of the cell when subjected to environmental variations, especially at the low voltages. A more practical model is shown in Figure 4, where the series resistance represents the PV cells internal circuit resistance, while parallel resistance is inversely related with leakage current to the ground. Usually, the series resistance is very small, which arises from the ohmic contact between metal and semiconductor internal resistance. But shunt resistance is very large and represents the surface quality along the periphery, noting that in ideal case R_S is zero (0) and R_{sh} is infinity (∞) [19].

Figure 4: Equivalent model of single diode PV cell with series and shunt resistances [18].

Applying Kirchhoff's law to the node where, I_{Ph}, I_d, R_{Sh} and R_S meet, the following output current can be deduced:

$$I_{PV} = I_{Ph} - I_d - I_{R_{Sh}} \tag{8}$$

Where,

$$I_d = I_S \left[\exp\left(\frac{V + I_{PV}R_S}{nV_T} \right) - 1 \right] \tag{9}$$

$$I_{R_{Sh}} = \frac{V + I_{PV}R_S}{R_{Sh}} \tag{10}$$

$I_{R_{Sh}}$ = Shunt/parallel resistance current,

therefore,

$$I_{PV} = I_{Ph} - I_S \left[\exp\left(\frac{q(V+I_{PV}R_S)}{nKT_c} \right) - 1 \right] - \frac{V+I_{PV}R_S}{R_{Sh}} \tag{11}$$

For PV module,

$$I_{PV} = I_{Ph} - I_S \left[\exp\left(\frac{q(V+I_{PV}R_S)}{nN_sKT_c} \right) - 1 \right] - \frac{V+I_{PV}R_S}{R_{Sh}} \tag{12}$$

Where,

N_s = Number of series connected cells

This model yields more accurate results than the R_S-model, but at the expense of longer computational time [20].

However, the photocurrent mainly depends on the solar irradiance and cell's operating temperature, expressed as:

$$I_{Ph} = [I_{Sc} + K_i(T_c - T_{nom})]\frac{G}{G_{nom}} \tag{13}$$

I_{Sc} = Short circuit current at standard test condition,
K_i = Cell's short circuit current temperature coefficient,
T_{nom} = Nominal temperature,
T_c = Cell's operating temperature,
G = Solar irradiance in W/m^2, and
G_n = Nominal solar irradiance in W/m^2,

The saturation current varies as a cubic function of temperature [6], which is represented as;

$$I_S = I_{rs} \left[\frac{T_{nom}}{T_c} \right]^3 \exp\left[\frac{qE_g}{nK} \left(\frac{1}{T_{nom}} - \frac{1}{T_c} \right) \right] \tag{14}$$

Where,

I_{rs} = Cell's reverse saturation current at nominal temperature and solar radiation,
E_g = Band-gap energy of the silicon solar cell = 1.12eV, and
n = Ideality factor.

The reverse saturation current can be further improved as a function of temperature as follows;

$$I_{rs} = \frac{I_{Sc}}{\exp\left(\frac{qV_{OC}}{nNsKT_C} \right) - 1} \tag{15}$$

Where,

V_{OC} = Open circuit voltage
I_{Sc} = Short circuit current.

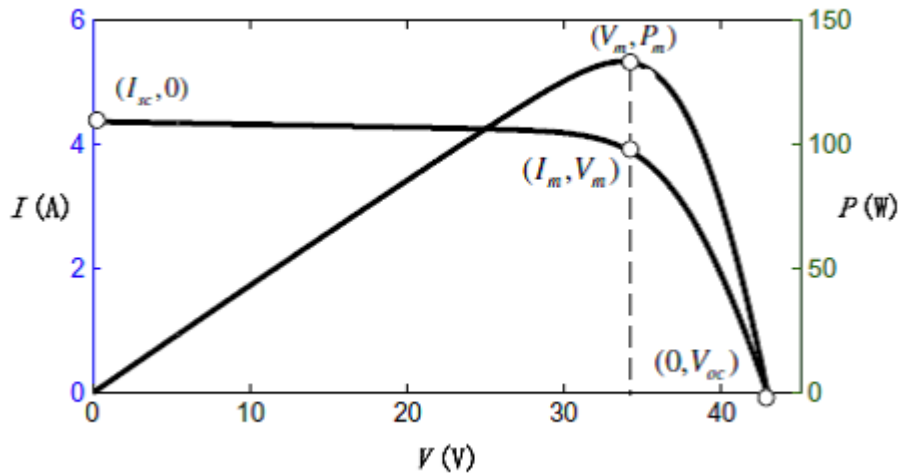➤ *PV cell I-V characteristics*

Figure 5: I-V and P-V characteristic curve of a PV module [21]

1. Short circuit current, I_{SC}: It refers to the maximum current produced by cell under given conditions of light and temperature corresponding to zero output voltage. The power at this point is zero.

2. Open circuit voltage, V_{OC}: It refers to the maximum voltage from the cell under given conditions of light and temperature corresponding to maximum voltage potential but zero current flow. The power at this point is also zero.

$$V_{OC} = \frac{nKT_C}{q} \ln\left[\frac{I_{Ph}}{I_S} + 1\right] \tag{16}$$

3. Current at maximum power, I_{MP}: It refers to the current that results in maximum power under given conditions of light and temperature and it is used as the rated current of a cell.

4. Voltage at maximum power, V_{MP}: It refers to the voltage that results in maximum power under given conditions of light and temperature and is used as the rated voltage of a cell.

5. Fill factor (FF): The fill factor, also known as the curve factor as shown in Figure 5, is a measure of sharpness of the knee in an I-V curve. It indicates how well a junction was made in the cell and how low the series resistance has been made. It can be lowered by the presence of series resistance and tends to be higher whenever the open circuit voltage is high. The maximum value of the fill factor is obviously less than one.

$$FF = \frac{P_{Max}}{V_{OC} \times I_{SC}} = \frac{V_{Max}}{V_{OC}} \times \frac{I_{Max}}{I_{SC}} \tag{17}$$

Other than the above, the two other important parameters that influence the characteristics of solar cells are the solar irradiance, an instantaneous quantity describing the rate of solar radiation (power) incident on a surface and solar insolation referring to the amount of solar energy received on a surface.

6. Maximum power point P_M,: This is the point of intersection between I_{MP} and V_{MP} as shown in Figure 5.

Solar cell efficiency

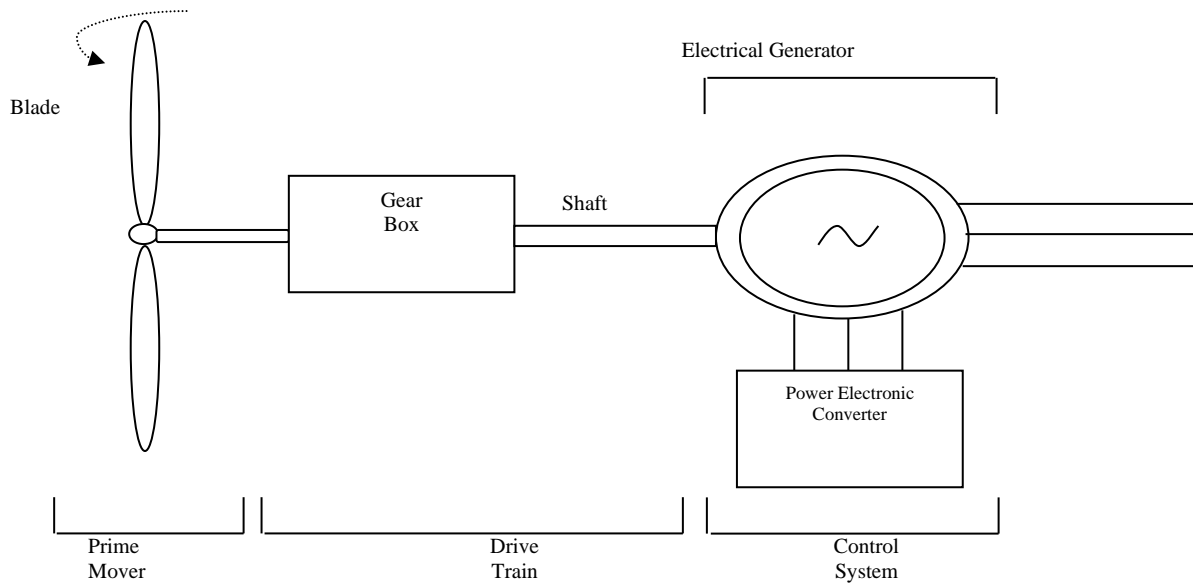The solar cell power conversion efficiency can be given as:

$$\eta_{ec} = \frac{P_{max}}{P_{in}} = \frac{V_{Max} \times I_{Max}}{\text{incident solar radiation} \times \text{area of solar cell}} \tag{18}$$

Thus,

$$\eta_{ec} = \frac{P_{max}}{P_{in}} = \frac{V_{max} I_{max}}{A. G_{in}} \tag{19}$$

Where, I_{Max} and V_{Max} are the current and voltage for maximum power, corresponding to solar irradiance G_{in}.

2.2.2   Wind turbine mathematical modeling

Figure 6: A Typical wind turbine assembly

The wind turbine is designed to capture the kinetic energy present in wind and convert it to electrical energy. From a modeling point of view, a typical wind turbine consists of the following components:

- Prime mover (turbine rotor and blade assembly)
- Drive train (shaft and gear box)
- Electrical generator (an induction generator is preferred over the synchronous choice because of its ability to withstand frequent variations in speed)
- Control system

The interaction between these components determines how much kinetic energy extractable from the wind. Modeling of the electrical subsystem is fairly straight forward based on the fact that most simulation software includes a built-in induction/synchronous generator model. However, modeling of the aerodynamics and mechanical drive train is more challenging because their models are based on the differential and algebraic equations that describe their operation [22]. For the purpose of this study, both the electrical and aerodynamic models of wind turbine were considered with special attention on the relationship between wind speed and extractable power; real and reactive power response to load and the simulation and results were carried out with the aid of MATLAB software.

- *Aerodynamic model*

The extractable power from the wind depends on the interaction between the wind turbine rotor and the wind speed. However, the fundamental equation governing the power available in the wind is given by:

$$P_{wind} = \frac{1}{2}\rho AV_w^3 \tag{20}$$

Where,
ρ = Air density (kg/m^3)
A = Area swept by rotor blades (m^2)
V_w = Average wind speed (m/s)

Also, according to Betz, the maximum power extractable by an ideal turbine rotor with infinite blades from wind under ideal conditions is 59.26% of the power available in the wind. This limit is known as the Betz limit [23]. In practice, wind turbines are limited to two or three blades due to a combination of structural and economic considerations, and hence, the amount of power they can extract is closer to about 50% of the available power [24]. Thus, the ratio of extractable power to available power can be expressed as:

$$C_P = \frac{\text{Extractable Power}}{\text{Available Power}} \tag{21}$$

From equation (21),

Extractable power, P_{wind} is

$$P_{wind} = \frac{1}{2} C_P \rho A V_w^3 \tag{22}$$

Also, the delivered power, P_e is given as;

$$P_{wind} = \frac{1}{2} C_P \rho A V_w^3 N \tag{23}$$

Where,

N is the combined efficiency of the gearbox and alternator.

C_P is expressed as a function of tip-speed rotor (λ) and blade pitch angle β.

It is given as;

$$C_P(\lambda, \beta) = \frac{1}{2}\left[\frac{116}{\lambda_1} - 0.4\beta - 5\right]\exp^{\frac{-21}{\lambda_1}} + 0.0068\lambda \tag{24}$$

Where,

$$\lambda_1 = \left[\frac{1}{\frac{1}{\lambda + 0.08\beta} - \frac{0.035}{\beta^3 + 1}}\right] \tag{25}$$

$$\lambda = \frac{\Omega R}{V_w} \tag{26}$$

C_P = Wind turbine power coefficient

λ = Tip-speed ratio

λ_1 = Constant

For the purpose of this study C_P is taken to be 0.48 owing to the fact that the wind turbine data used has only 3 blades.

3. Results and Discussion

3.1 PV Module Simulation Results

The results of PV module simulation under varying temperature and irradiance conditions obtained are based on the parameters extracted from Mitsubishi Electric PV panel manufacturer's datasheet used.

3.1.1 Temperature variation simulation results

The following graphs show the effect of temperature on PV module of ideal and non-ideal single diode models at different temperature values of 25, 30, 35, 40 and 45°C subject to constant irradiance value of $1000W/m^2$.

The Figures 7-10 show the I-V and P-V characteristics of an ideal and non-ideal single diode PV module models for varying temperature, T respectively. It is evident from these simulation results that the current generated by the incident light remained virtually constant while the voltage decreases significantly in value for every increase in temperature. Also, the power decreases as voltage decreases. However, a great similarity exists between the Ideal and non-ideal PV module models under temperature variations. In addition, it may be said that increment in temperature causes decrement in the value of both maximum power voltage (V_{mp}) and maximum power current (I_{mp}). Also, the simulation result shows that the short-circuit current is independent of temperature rise for the models under study.
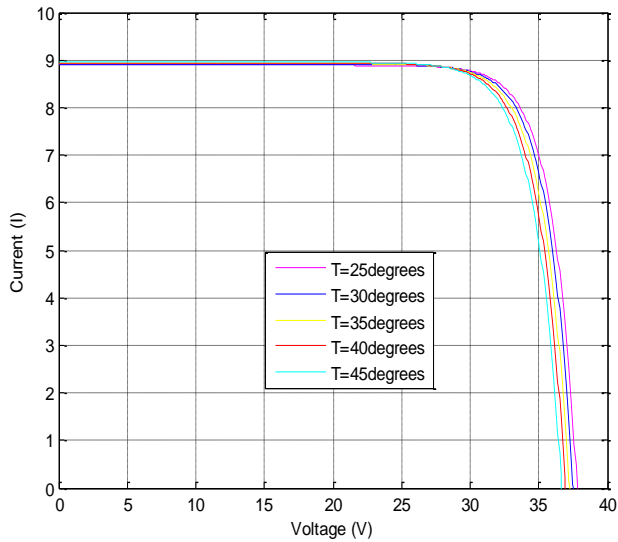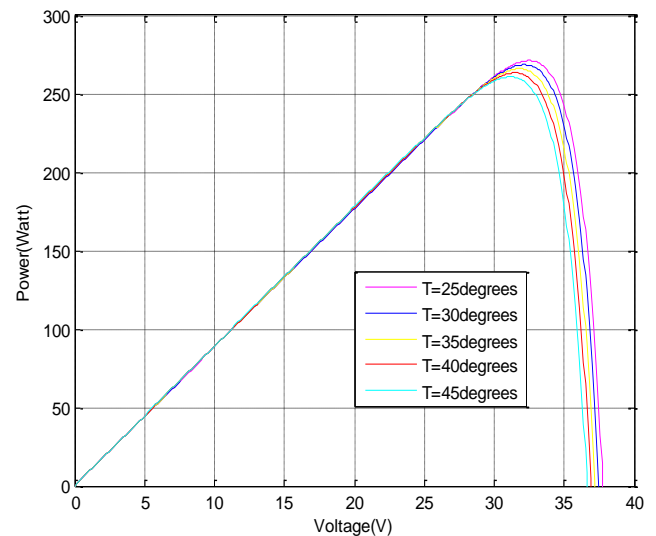

Figure 7: Current-voltage (I-V) characteristics of an ideal PV module under varying temperature (℃) condition
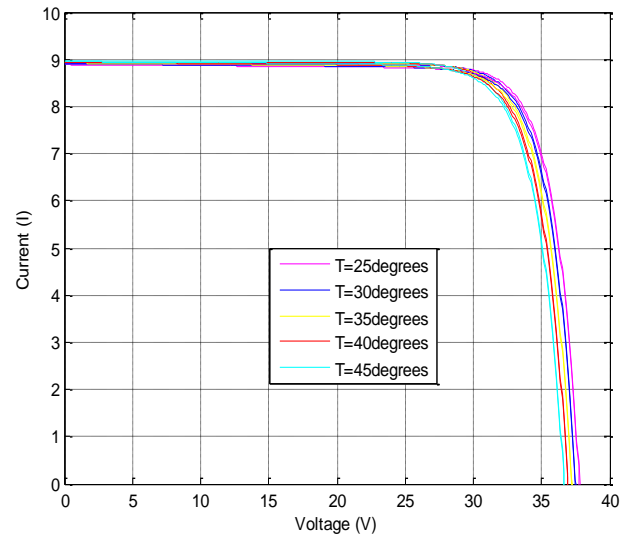
Figure 9: Current-voltage (I-V) characteristics of a non-ideal PV module under varying temperature (℃) condition
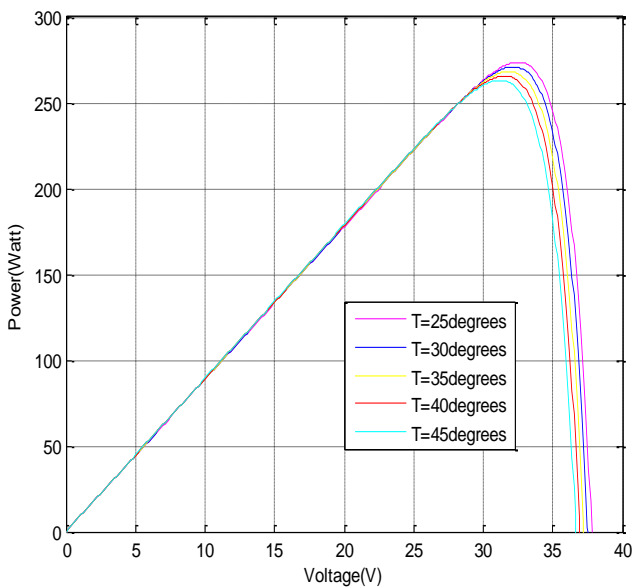
Figure 8: Power-voltage (P-V) characteristics of an ideal PV module under varying temperature (℃) condition
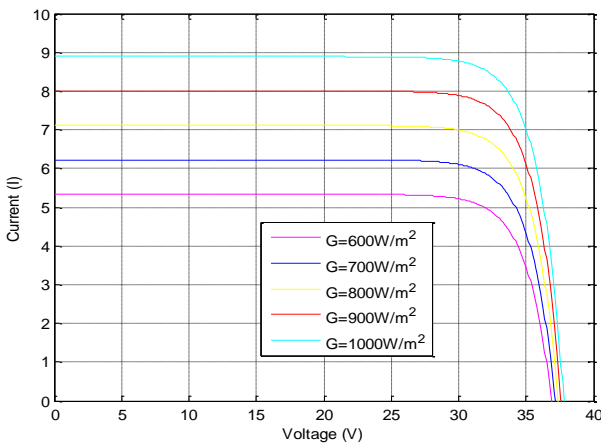

Figure 10: Power-voltage (P-V) characteristics of a non- ideal PV module under varying temperature (℃) condition

3.1.2 Irradiance variation simulation results

Figures 11-14 show the simulation result of single diode model of PV module under varying irradiance (G) values of 600W/m², 700W/m², 800W/m², 900W/m²and 1000W/m² respectively subject to constant temperature of 25℃. These show that the effect of irradiance is much high in the short circuit current than in the open circuit voltage for the I-V characteristics. Also, the effect of irradiance variation on P-V characteristics shows that increase in irradiance causes significant increase in the generated voltage.

However, the model results show few variations in the values of short circuit current (I_{sc}), open circuit voltage (V_{oc}), maximum power voltage (V_{mp}), maximum power current (I_{mp}), maximum power (P_{max}), fill factor (F), and efficiency (η) for both ideal and non-ideal PV cell with single and double diode models when subjected to different irradiance values. This indicates solid performance of a PV cell.
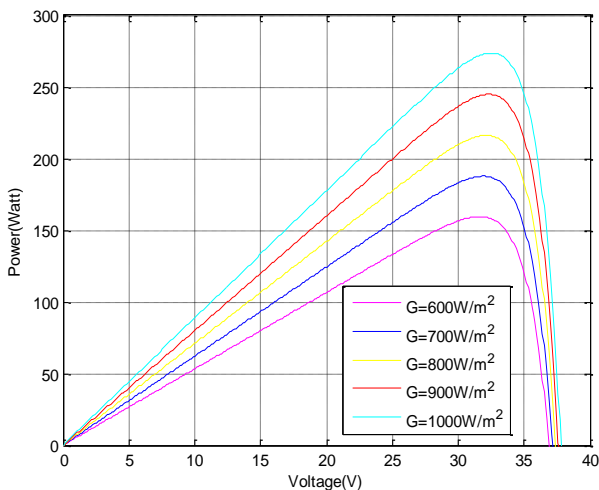

Figure 11: Current-voltage (I-V) characteristics of an ideal single diode PV module model under varying irradiance condition
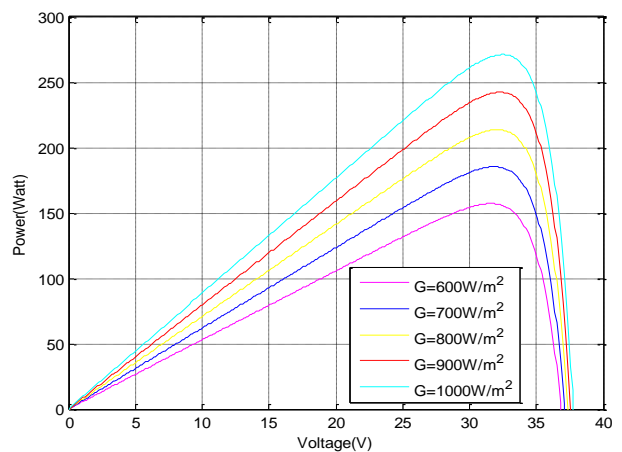
module model under varying irradiance condition
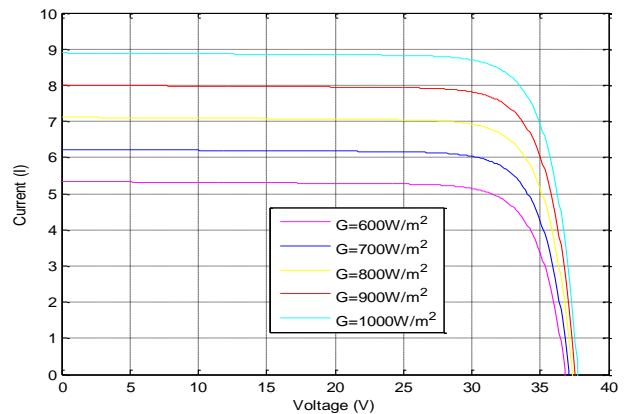
Figure 13: Current-voltage (I-V) characteristics of a non-ideal single diode PV module model under varying irradiance condition

Figure 12: Power-voltage (P-V) characteristics of an ideal single diode PV

Figure 14: Power-voltage (P-V) characteristics of an ideal single diode PV

**module model under varying irradiance
condition**

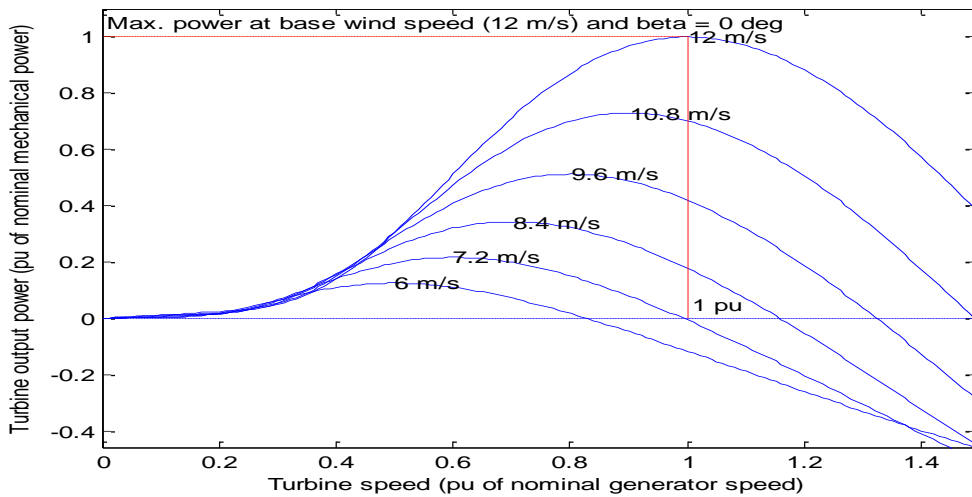*3.2 Wind Turbine Simulation Result*

Figure 15 shows the simulation result of wind turbine power characteristics under different wind speed. It is evident from Figure 15 that increase in speed causes significant increase in the generated turbine output power. However, the maximum power for each operating wind speed occurred at pitch angle, β = 0°.

**Figure 15: Wind turbine power and speed characteristics (pitch angle beta = 0^0)**

*3.3 Hybrid Solar-Wind Simulation Results*

Figure 16 shows the output power response of a hybrid solar-wind power system under varying wind velocity at constant temperature of 25 degrees and irradiance of $1000W/m^2$. However, it is evident from the result that increase in wind velocity causes increase in the cumulative output of the combined Solar-Wind power system.
Also, Figure 17 shows the output power response of a hybrid solar-wind power system under varying irradiance at constant temperature of 25 degrees and wind velocity of $12m/s^2$. However, it is evident from the result that increase in irradiance causes significant increase in the cumulative output of the combined solar-wind power system.

More so, Figure 18 shows the output power response of a hybrid solar-wind power system under varying temperature conditions at constant irradiance of $1000W/m^2$ and wind velocity of $12m/s^2$. However, it is evident from the result that increase in temperature causes significant decrease in the cumulative output of the combined solar-wind power system.
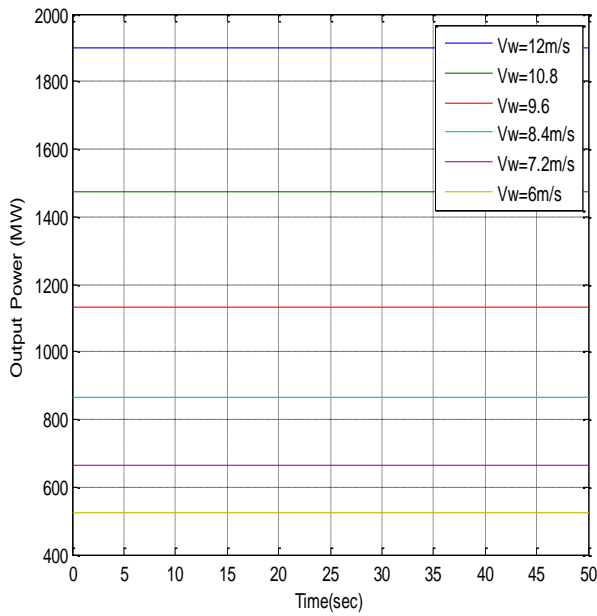
Figure 16: Hybrid output power (MW) response under varying wind velocity
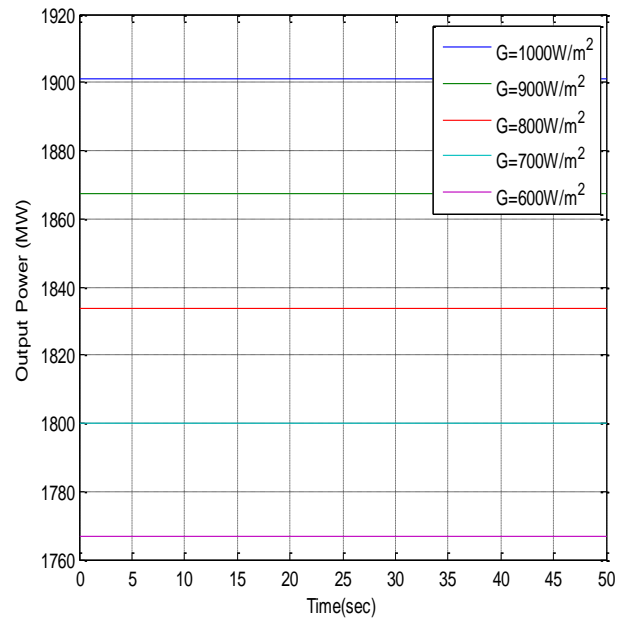
Figure 17: Hybrid output power (MW) response under varying irradiance
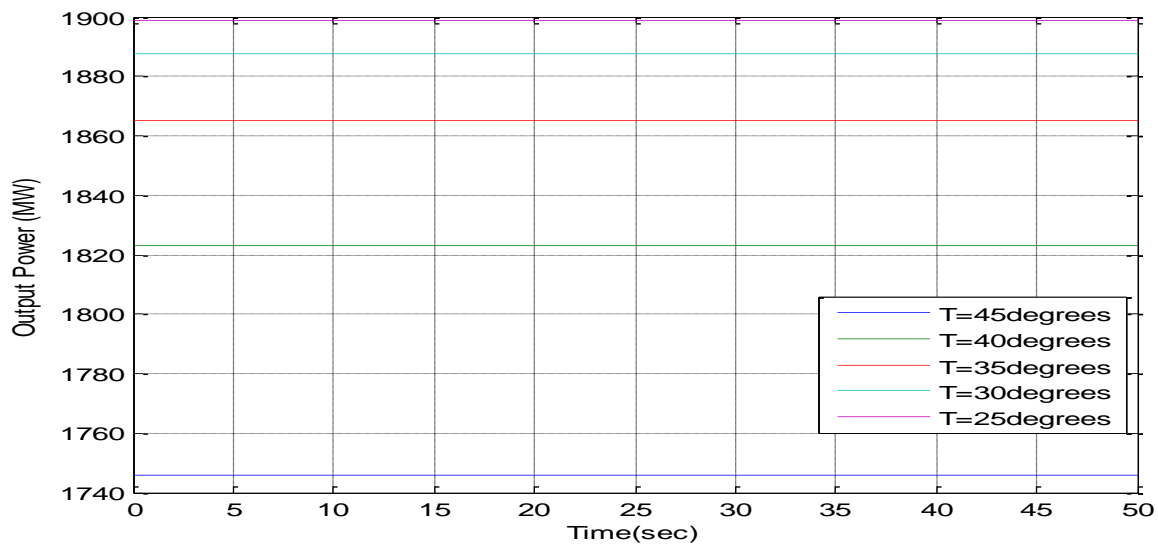
Figure 18: Hybrid output power (MW) response under varying temperature

4. Conclusion

In this research, a comprehensive fundamental modeling of hybrid renewable solar-wind power generation with special attention on studying the effect of environmental changes on the system. The equivalent circuit model for the individual subsystems; PV module, wind turbine and the combined system were discussed. The result of temperature effect studies on both the ideal and non-ideal single diode models of PV Module shows that increase in temperature causes decrease in the maximum power output of the Module under constant irradiance condition. A comparison between

the ideal and non-ideal PV module models demonstrated that the non-ideal single diode model offers a more realistic behavior under different varying environmental conditions. More so, the results from the aerodynamic modeling and simulation of the wind turbine under study shows that increase in wind speed causes increase in power but when the wind speed is increased above the turbine's rated wind speed, the output power begins to decline.

In addition, the results of hybrid solar-wind power system simulation show a geometrical increase in power output when compared to the individual subsystems. Also, its performance evaluation under different varying environmental factors shows that increase in irradiance and wind velocity has a more significant impact on the hybrid system than temperature changes.

However, the individual subsystems of the proposed hybrid renewable solar-wind power generation as well the combined system have been modeled and simulated, and their performance under different environmental condition obtained so as to help operators or users know what is to be generated at every environmental condition.

References

[1] K. Sandeep and G. Vijay (2013). Hybrid System of PV Solar / Wind /Fuel Cell. International Journal of Advanced Research in Electrical, Electronics and Instrumentation Engineering (IJAREEIE), Vol. 2(8), pp. 3666-3679.

[2] A. O. Phebe and A. S. Samuel (2016). A Review of Renewable Energy Sources, Sustainability Issues and Climate Change Mitigation. Cogent Engineering, Vol. 2016(3), pp. 1-14.

[3] H. Mahabub and B. M. Oishe (2015). Performance Analysis and Feasibility Study of Solar-Wind-Diesel Hybrid Power System in Rural Areas of Bangladesh. International Journal of Engineering Research and General Science, Vol. 3(5), pp. 410-420.

[4] M. D. Ibrahim, K. Abul and S. Ansari (2015). A Review of Hybrid Renewable Energy System for Electric Power Generation. International Journal of Engineering Research and Application (IJERA), Vol. 5(8), pp. 42-48.

[5] R. Avtar, N. Sahu, A. K. Aggarwal, S. Chakraborty, A. Kharrazi, A. P. Yunus, J. Dou and T. A. Kurniawan (2019). Exploring Renewable Energy Resources Using Remote Sensing and GIS—A Review. *Resources,* Vol. 2019(8), pp. 1-23.

[6] B. Binayak, R. P. Shiva, L. Kyung-Tae and A. Sung-Hoon (2014). Mathematical Modeling of Hybrid Renewable Energy System: A Review on Small Hydro-Solar-Wind Power Generation. International Journal of Precision Engineering and Manufacturing-Green Technology, Vol. 1(2), pp. 157-173.

[7] B. Jozsef, S. Tihamer-Tibor and B. Blanka (2018). Evaluation of Renewable Energy Sources in Peripheral Areas and Renewable Energy-Based Rural Development. Renewable and Sustainable Energy Reviews, Vol. 90, pp. 516 – 535.

[8] N. Swati and M. Lini (2014). Hybrid Renewable Energy: A Review. International Journal of Electronic and Electrical Engineering, Vol. 7(5), pp. 535-542.

[9] F. Glayoor, A. G. Swanson and H. Sibanda (2021). Optimizing sizing for a grid-connected hybrid renewable energy system: A case study of the residential sector in Duban, South Africa. Journal of Energy in Southern Africa. Vol. 32(4), pp. 11-27.

[10] M. Bashir and J. Sadeh (2011). Size Optimization of New Hybrid Stand-alone Renewable Energy System Considering a Reliability Index. Conference Paper January 2011. https://www.researchgate.net/publication/215955064.

[11] L. T. Clausen and D. Rudolph (2020). Renewable Energy for Sustainable Rural Development: Synergies and Mismatches. Energy Policy, Vol. 138, pp. 1-10.

[12] L. O. Aghenta and M. T. Iqbal (2019). Design and Dynamic Modeling of a Hybrid Power System for a House in Nigeria. International Journal of Photo Energy, Vol. 2019, pp. 1-13.

[13] Z. Teng, G. Ragigul and S. Kai (2021). Hybrid Data-Driven and Mechanistic Modeling Approaches or Multiscale Material and Process Design. Elsevier Engineering, Vol. 7, pp. 1231-1238.

[14] F. Bourennani, S. Rahnamayan and G. F. Naterer (2015). Optimal Design Methods for Hybrid Renewable Energy Systems. *International Journal of Green Energy, Vol. 12*, pp. 148-159.

[15] J. B. Fulzele and M. B. Daigavane (2018). Designe and Optimization of Hybrid PV-Wind Renewable Energy System. Materials Today Proceedings, Vol. 5(1), pp.810-818.

[16] E. Omorogiuwa and P. I. Obi (2020). Review on Modern Trends on Smart Remote Models for Monitoring PV System. World Journal of Engineering Research and Technology (WJERT). Vol. 6(2), pp. 54-65. www.wjert.org.

[17] M. Azzouzi, L. Mazzouz and D. Popescu (2014). Matlab-Simulink of Photovoltaic System Based on a Two-Diode Model. Proceedings of the World Congress on Engineering (WCE), 2nd – 4th July, 2014, London, U.K, pp. 328-333.

[18] I. Kashif, S. Zainal and T. Hamed (2011). Accurate MATLAB Simulink PV System Simulator Based on a Two-Diode Model. Journal of Power Electronics, Vol. 11(2), pp. 179-187.

[19] J. Abdul, A. Nazar and A. Omega (2012). Simulation on Maximum Power Point Tracking of the Photovoltaic Module using LabVIEW. International Journal of Advanced Research in Electrical, Electronics and Instrumentation Engineering (IJAREEIE), Vol. 1, pp. 190-199.

[20] A. E. Wafaa, M. A. E. Ashraf and A. E. S. S. Fouad (2013). Mathematical Model for Photovoltaic Cells. Leonard Journal of Sciences, Vol. 23, pp.13-28.

[21] Y. Jiang, J. A. Qahouq and M. Orabi (2011). Matlab/Pspice Hybrid Simulation Modeling of Solar PV Cell/Module. *2011 Twenty-Sixth Annual IEEE Applied Power Electronics Conference and Exposition (APEC)*, pp. 1244-1250.

[22] P. Srikanth and A. S. Sekhar (2015). Dynamic Analysis of Wind Turbine Drive Train Subjected to Non-Stationary Wind Load Excitation. Journal of Mechanical Engineering Science, Vol. 229(3), pp. 429-446.

[23] M. H. Ranjbar, S. A. Nasrazadani, H. Z. Kia and K. Gharali (2019). Reaching the betz Limit Experimentally and Numerically. Energy Equipment and Systems, Vol. 7(3), pp. 271-278.

[24] S. Mohit and S. Surya (2011). Dynamic Models for Wind Turbines and Wind Power Plants. National Renewable Energy Laboratory (NREL), pp. 9-18.

Appendix

Table A1: Pika T701 wind turbine installation and service manual

Parameter	Value
Turbine Type	3-blade HAWT, upwind free yaw
Rotor diameter	3.016 m
Swept area	7.01 m2
Blade type	Optimum twist-taper injection-molded glass-reinforced polypropylene resin
Speed control	Digitally-controlled alternator torque
Redundant control	One-shot centripetal overspeed brake
Tower top mass	45 kg
Rated power (approx.)	1500W @ 11 m/s
Annual output (approx.)	2,420 kWh at 5 m/s avg. (Rayleigh)
Cut-in wind speed	3.3 m/s
Survival wind speed	60 m/s
Turbine electrical output	REbus™ DC nanogrid: regulated +/-190VDC
Electrical parameters	**Nominal (Maximum)**
RE bus Power	1575 W (1785 W)
RE bus voltage	380 V (420 V)
RE bus current	4.7 A (6.7 A)

Table A2: Mitsubishi electric PV module datasheet

Mitsubishi Electric Photovoltaic Module Specification Sheet	
Manufacturer	Mitsubishi Electric
Model name	PV-MLU255HC
Cell type	Monocrystalline Silicon, 78mmx156mm
Number of cells	324cells
Maximum power rating (Pmax)	255Wp
Warranted minimum Pmax	247.4Wp
PV USA test condition rating (PTC)	230.5Wp
Open circuit voltage (Voc)	37.8V
Short circuit current (Isc)	8.89
Maximum power voltage (Vmp)	31.2V
Maximum power current (Imp)	8.18A
Module efficiency	15.40%
Aperture efficiency	16.70%
Tolerance of maximum power rating	+3/-3%
Static load test passed	5,4000Pa
Number of bus bars per cell	4Bus bars
Normal operating cell temperature (NOCT)	45.7℃
Maximum system voltage	DC 600V
Fuse rating	15A
Dimensions	64x40.1x1.81inch
Weight	44lbs (20kg)
Number of modules per pallet	20
Number of modules per container (40ft. Container)	560
Certifications	IEC 61215 2nd Edition, UL1703
Fire rating	Class C
Mitsubishi Electric Photovoltaic Module Specification Sheet	
Manufacturer	Mitsubishi Electric
Model name	PV-MLU255HC
Cell type	Monocrystalline Silicon, 78mmx156mm
Number of cells	324cells
Maximum power rating (Pmax)	255Wp
Warranted minimum Pmax	247.4Wp
PV USA test condition rating (PTC)	230.5Wp
Open circuit voltage (Voc)	37.8V
Short circuit current (Isc)	8.89
Maximum power voltage (Vmp)	31.2V
Maximum power current (Imp)	8.18A

Module efficiency	15.40%
Aperture efficiency	16.70%
Tolerance of maximum power rating	+3/-3%
Static load test passed	5,4000Pa
Number of bus bars per cell	4Bus bars
Normal operating cell temperature (NOCT)	45.7℃
Maximum system voltage	DC 600V
Fuse rating	15A
Dimensions	64x40.1x1.81inch
Weight	44lbs (20kg)
Number of modules per pallet	20
Number of modules per container (40ft. Container)	560
Certifications	IEC 61215 2nd Edition, UL1703
Fire rating	Class C